

NUMERICAL SIMULATION OF SINGLE SPECIES DOPANT DIFFUSION IN SILICON UNDER EXTRINSIC CONDITIONS

J. Lang and W. Merz*

Konrad-Zuse-Zentrum für Informationstechnik Berlin, Takustr. 7, 14195 Berlin-Dahlem, Germany

*Technische Universität München, Dachauer Str. 9a, 80335 München, Germany

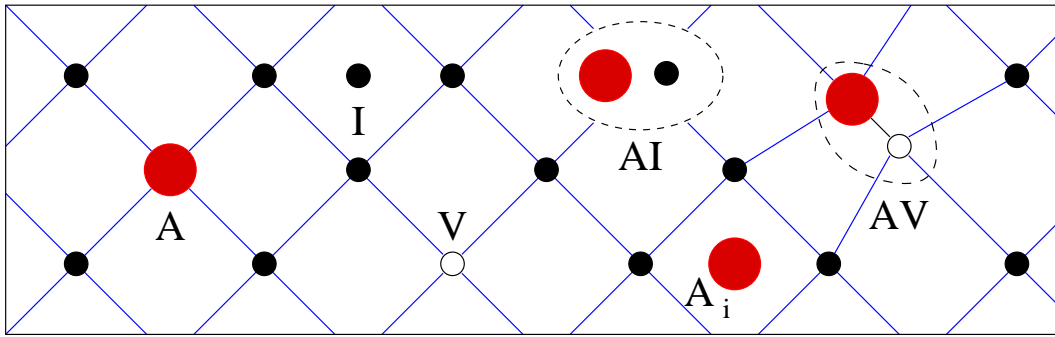
Abstract

In this article we consider a general model for phosphorus diffusion in silicon under extrinsic doping conditions. At such high concentrations we have to include the charged species and the internal electric field of the crystal, both of which can have profound effects on diffusion. In principle, this leads to a very large number of drift-diffusion-reaction equations: one for each charge state of every species, plus one Poisson equation to describe the internal electric field (in terms of the electron/hole concentration). The number of equations can be reduced substantially by making additional assumptions on the distribution of charge states and local equilibrium assumptions concerning the reaction terms. The resulting model turns out to be very interesting for numerical investigation. We solve the problem numerically in two space dimensions with the adaptive finite element program KARDOS and describe the numerical method used here to treat the resulting drift-diffusion-reaction problem.

1 Introduction

At the heart of modern silicon technology lies the doping process, where impurity atoms of higher or lower chemical valence as silicon, such as Arsenic, Phosphorus and Boron, are introduced into a silicon crystal to influence its electrical properties. Such dopants diffuse under high temperatures (900–1200⁰C) with an unusual mechanism, the so-called *pair diffusion* mechanism. A detailed and up-to-date description can also be found in [5].

Usually, dopant atoms occupy substitutional sites in the silicon crystal lattice, losing (donors such as Arsenic and Phosphorus) or gaining (acceptors such as Boron) by this an electron. We denote such *substitutional defects* by A . An “ordinary” diffusion mechanism involving direct interchange with neighbouring silicon atoms turns out to be energetically unfavourable, see [5]. Instead, the dopants diffuse by interacting with native *point defects* called interstitials and vacancies, which we denote by I and V , respectively. *Interstitials* are silicon atoms which are not placed on a lattice site and move through the crystal unconstrained, and *vacancies* are empty lattice sites. Both can form *mobile pairs* with dopant atoms, designated by AI and AV as depicted in the scheme below.



Scheme of pair diffusion.

There is no general consensus on the *exact* nature of the mechanism for pair mobility. One way to visualize it is as follows: in the case of AI -pairs, an interstitial and a dopant atom share a lattice site called an *interstitialcy*. The dopant can now “change partners” by moving through an intermediate interstitial stage (denoted by A_i). On the other hand, dopants and vacancies exhibit a certain affinity. So, a vacancy near a dopant moves around this dopant quickly, and an occasional interchange between dopant and vacancy leads to a random walk effect.

This “pair diffusion mobility” mechanism is supported by a majority of authors, see for instance [3,7,11,17,18]; alternative models can be found in [8,9], where dopants are admitted to diffuse. One minor alternative is to consider mobile interstitial dopants A_i as the diffusing species rather than mobile pairs AI . However, as can be seen from the above remark, this distinction makes no real difference, and, moreover, it has no meaning for the treatment that follows, so we shall stick to the pair description here.

The paper is arranged as follows:

In the next section we formulate the derivation of a general model for dopant diffusion following the ideas of [7] and [11]. Under extrinsic doping conditions we have to take into account different charged states of the involved species, such as dopants, defects and created pairs. This results in a large number of equations and consequently in many physical parameters, which are usually unknown. In order to reduce the number of equations we make assumptions concerning the distribution of the charge states and assume local equilibrium in the chemical reactions. As we will see below, the resulting model consists of five drift–reaction–diffusion equations, plus an elliptic equation for the electrical field.

In section three this system of equations will be treated numerically in two spatial dimensions. The simulation of the present dopant diffusion model requires the numerical solution of systems of time–dependent partial differential equations involving algebraic equations as well. These problems belong to the class of complex problems due to highly nonuniformity of information distributed in space and time. In such a situation adaptive algorithms which have been a topic of continuing investigations during the last years are often the only way to get an accurate solution with an acceptable amount of computational time and memory requirement. In contrast to the widely used method of lines approach we apply the adaptive Rothe method based on the discretization sequence first in time and then in space [1,14]. This allows us to adapt the spatial discretization in each time step employing directly a multilevel finite element solver [2,4]. The time discretization is done by a linearly implicit method of Rosenbrock type with an automatic step size control.

The whole algorithm was implemented in the program package KARDOS which is now an efficient and robust code to simulate a wide range of complicated evolution problems.

2 Diffusion under Extrinsic Conditions

2.1 Formulation of the Model

As announced at the beginning, we will turn our attention to the case of *extrinsic doping conditions* in the following, i.e., we will consider silicon crystals where

$$C_A \gg n_i,$$

n_i being the intrinsic carrier concentration and C_A denotes the concentration of the dopant in the crystal. This assumption forbids the neglect of the charges of dopants and pairs for several reasons which will be clarified below.

The charge state of the species will be denoted by superscripts included in parentheses. For the interstitials we consider the charge states

$$I^{(i)}, \quad i = -1, 0, +1,$$

and for the vacancies

$$V^{(j)}, \quad j = -2, -1, 0, +1, +2.$$

The unpaired dopant on a lattice site, phosphorus in our case, has always the fixed charge state $A^{(q)}$, $q = +1$. So the pairs under consideration are

$$(AI)^{(q+i)} \quad \text{and} \quad (AV)^{(q+j)}.$$

Next, we state the set of reactions between the species and formulate the reaction rates R (supplied with appropriate indices) in terms of concentrations C_Y^z , where $Y = I, V, AI, AV, A$, and z denoting the charge state. We consider

- dopant–defect pairing:

$$\begin{aligned} A^{(q)} + I^{(i)} &\rightleftharpoons (AI)^{(q+m)} + (m-i)n, \\ R_{A,I}^{im} &= k_{A,I}^{im} C_A^q C_I^i - \tilde{k}_{A,I}^{im} C_{AI}^{q+m} \left(\frac{n}{n_i} \right)^{m-i}, \end{aligned} \quad (2.1)$$

$$\begin{aligned} A^{(q)} + V^{(j)} &\rightleftharpoons (AV)^{(q+r)} + (r-j)n, \\ R_{A,V}^{jr} &= k_{A,V}^{jr} C_A^q C_V^j - \tilde{k}_{A,V}^{jr} C_{AV}^{q+r} \left(\frac{n}{n_i} \right)^{r-j}, \end{aligned} \quad (2.2)$$

- defect recombination:

$$(AI)^{(q+i)} + V^{(j)} \rightleftharpoons A^{(q)} - (i+j)n,$$

$$R_{AI,V}^{ij} = k_{AI,V}^{(q+i)j} C_{AI}^{q+i} C_V^j - \tilde{k}_{AI,V}^{(q+i)j} C_A^q \left(\frac{n}{n_i} \right)^{-i-j}, \quad (2.3)$$

$$(AV)^{(q+j)} + I^{(i)} \rightleftharpoons A^{(q)} - (i+j)n,$$

$$R_{AV,I}^{ji} = k_{AV,I}^{(q+j)i} C_{AV}^{q+j} C_I^i - \tilde{k}_{AV,I}^{(q+j)i} C_A^q \left(\frac{n}{n_i} \right)^{-i-j}, \quad (2.4)$$

- Frenkel pairs:

$$I^{(i)} + V^{(j)} \rightleftharpoons -(i+j)n,$$

$$R_{I,V}^{ij} = k_{I,V}^{ij} C_I^i C_V^j - \tilde{k}_{I,V}^{ij} \left(\frac{n}{n_i} \right)^{-i-j}, \quad (2.5)$$

- ionization of the defects:

$$I^{(i)} \rightleftharpoons I^{(l)} + (l-i)n,$$

$$R_I^{il} = k_I^{il} C_I^i - \tilde{k}_I^{il} C_I^l \left(\frac{n}{n_i} \right)^{l-i}, \quad (2.6)$$

$$V^{(j)} \rightleftharpoons V^{(k)} + (k-j)n,$$

$$R_V^{jk} = k_V^{jk} C_V^j - \tilde{k}_V^{jk} C_V^k \left(\frac{n}{n_i} \right)^{k-j}, \quad (2.7)$$

- ionization of the pairs:

$$(AI)^{(q+i)} \rightleftharpoons (AI)^{(q+l)} + (l-i)n,$$

$$R_{AI}^{il} = k_{AI}^{il} C_{AI}^{q+i} - \tilde{k}_{AI}^{il} C_{AI}^{q+l} \left(\frac{n}{n_i} \right)^{l-i}, \quad (2.8)$$

$$(AV)^{(q+j)} \rightleftharpoons (AV)^{(q+k)} + (k-j)n,$$

$$R_{AV}^{jk} = k_{AV}^{jk} C_{AV}^{q+j} - \tilde{k}_{AV}^{jk} C_{AV}^{q+k} \left(\frac{n}{n_i} \right)^{k-j}, \quad (2.9)$$

where $m, l = -1, 0, +1$, $r, k = -2, -1, 0, +1, +2$, and the k (supplied with the respective indices) denote the forward reaction-rate constant, the \tilde{k} the reverse ones.

For each of the charged species we can now establish the corresponding balance equation taking into account the reaction terms (2.1)–(2.9). The fluxes for the mobile species, i.e.,

for $X = I, V, AI, AV$, are defined in terms of the concentrations

$$J_X^z = -D_X^z \left(\nabla C_X^z + z C_X^z \nabla \ln \left(\frac{n}{n_i} \right) \right).$$

Since $J_A^z = 0$, we get the well known sytem of equations

$$\frac{\partial C_I^i}{\partial t} + \text{div } J_I^i = - \sum_m R_{A,I}^{im} - \sum_j R_{AV,I}^{ji} - \sum_j R_{I,V}^{ij} - \sum_l R_I^{il} + \sum_l R_I^{li}, \quad (2.10)$$

$$\frac{\partial C_V^j}{\partial t} + \text{div } J_V^j = - \sum_r R_{A,V}^{jr} - \sum_i R_{AI,V}^{ij} - \sum_i R_{I,V}^{ij} - \sum_k R_V^{jk} + \sum_k R_V^{kj}, \quad (2.11)$$

$$\frac{\partial C_{AI}^{q+i}}{\partial t} + \text{div } J_{AI}^{q+i} = \sum_m R_{A,I}^{im} - \sum_j R_{AI,V}^{ij} - \sum_l R_{AI}^{il} + \sum_l R_{AI}^{li}, \quad (2.12)$$

$$\frac{\partial C_{AV}^{q+j}}{\partial t} + \text{div } J_{AV}^{q+j} = \sum_r R_{A,V}^{jr} - \sum_i R_{AV,I}^{ji} - \sum_k R_{AV}^{jk} + \sum_k R_{AV}^{kj}, \quad (2.13)$$

$$\frac{\partial C_A^q}{\partial t} = - \sum_{i,l} R_{A,I}^{il} - \sum_{j,k} R_{A,V}^{jk} + \sum_{i,j} R_{AI,V}^{ij} + \sum_{j,i} R_{AV,I}^{ji}. \quad (2.14)$$

The Poisson equation for the electrical field requires the balance of all charged species including the electrons n and the holes p , which is

$$\begin{aligned} -U_T \Delta \ln \left(\frac{n}{n_i} \right) &= \frac{e}{\varepsilon} \left(-n + p + q C_A^q + \sum_i i C_I^i + \sum_j j C_V^j \right. \\ &\quad \left. + \sum_i (q+i) C_{AI}^{q+i} + \sum_j (q+j) C_{AV}^{q+j} \right), \end{aligned} \quad (2.15)$$

where $U_T = k_B T / e$ is the thermal voltage, k_B is the Boltzmann constant, T the absolute temperature, ε denotes the dielectric constant and e is the elementary charge.

The just mentioned model consists of eighteen coupled equations containing a huge number of parameters. In order to reduce the parameters we introduce some conventional assumptions. We do not consider ‘‘intermediate’’ charge states of the pairs here, that means $m = i$ and $r = j$ in the reaction rates (2.1) and (2.2), respectively. Moreover, we assume equilibrium concerning the ionization, i.e., we state that

$$R_I^{il} = 0, \quad R_V^{jk} = 0, \quad R_{AI}^{il} = 0, \quad R_{AV}^{jk} = 0,$$

for all indices i, j, k, l . Consequently, we are now able to express each charge state in terms of the neutral one. Especially for the interstitials we get

$$I^{(i)} \rightleftharpoons I^{(0)} - in,$$

with the reaction rate

$$R_I^{(i0)} = k_I^{i0} C_I^i - \tilde{k}_I^{i0} C_I^0 \left(\frac{n}{n_i}\right)^{-i} = 0,$$

leading to

$$C_I^i = K_I^i \left(\frac{n}{n_i}\right)^{-i} C_I^0, \quad (2.16)$$

with the equilibrium constant $K_I^i = \tilde{k}_I^{i0}/k_I^{i0}$. For the remaining reactions (2.7)–(2.9) we get with the same idea

$$C_V^j = K_V^j \left(\frac{n}{n_i}\right)^{-j} C_V^0, \quad (2.17)$$

$$C_{AI}^{q+i} = K_{AI}^{q+i} \left(\frac{n}{n_i}\right)^{-i} C_{AI}^q, \quad (2.18)$$

$$C_{AV}^{q+j} = K_{AV}^{q+j} \left(\frac{n}{n_i}\right)^{-j} C_{AV}^q, \quad (2.19)$$

with the equilibrium constants K_V^j , K_{AI}^{q+i} and K_{AV}^{q+j} (note $K_X^0 = 1$), the definition of which in terms of forward and reverse reaction rates is obvious (the indices l and k vanish in the equilibrium case).

Employing again the abbreviation $X = I, V, AI, AV$, summation over all charge states z yields

$$C_X = \sum_z C_X^{\alpha+z} = \sum_z K_X^{\alpha+z} \left(\frac{n}{n_i}\right)^{-z} C_X^\alpha, \quad (2.20)$$

where $\alpha = 0$ for $X = I, V$, and $\alpha = q$ for $X = AI, AV$. Hence

$$C_X^\alpha = \frac{C_X}{\sum_z K_X^{\alpha+z} \left(\frac{n}{n_i}\right)^{-z}}.$$

Using (2.16)–(2.19) we end up with

$$C_X^{\alpha+z} = \frac{K_X^{\alpha+z} \left(\frac{n}{n_i}\right)^{-z} C_X}{\sum_z K_X^{\alpha+z} \left(\frac{n}{n_i}\right)^{-z}}. \quad (2.21)$$

So, it is easy to compute from the total concentrations C_I, C_V, C_{AI}, C_{AV} each charged state by means of the algebraic equation (2.21).

Next, the total flux is

$$J_X = \sum_z J_X^{\alpha+z} = - \sum_z D_X^{\alpha+z} \left(\nabla C_X^{\alpha+z} + (\alpha+z) C_X^{\alpha+z} \nabla \ln \left(\frac{n}{n_i} \right) \right). \quad (2.22)$$

We substitute (2.21) in (2.22) to get after some calculation

$$J_{\mathbf{X}} = -\mathcal{A}_{\mathbf{X}}(n) \left(\nabla C_{\mathbf{X}} + \mathcal{B}_{\mathbf{X}}(n) C_{\mathbf{X}} \nabla \ln \left(\frac{n}{n_i} \right) \right), \quad (2.23)$$

with the definitions

$$\mathcal{A}_{\mathbf{X}}(n) = \frac{\sum_z D_{\mathbf{X}}^{\alpha+z} K_{\mathbf{X}}^{\alpha+z} \left(\frac{n}{n_1} \right)^{-z}}{\sum_z K_{\mathbf{X}}^{\alpha+z} \left(\frac{n}{n_1} \right)^{-z}} \quad (2.24)$$

and

$$\mathcal{B}_{\mathbf{X}}(n) = \frac{\sum_z (\alpha + z) K_{\mathbf{X}}^{\alpha+z} \left(\frac{n}{n_1} \right)^{-z}}{\sum_z K_{\mathbf{X}}^{\alpha+z} \left(\frac{n}{n_1} \right)^{-z}}, \quad (2.25)$$

Note that the averaged quantities $\mathcal{A}_{\mathbf{X}}$ and $\mathcal{B}_{\mathbf{X}}$ depend on the electrical field.

Finally, we can write the complete set of the state equations in terms of the total concentrations

$$\frac{\partial C_{\mathbf{I}}}{\partial t} + \operatorname{div} J_{\mathbf{I}} = - \sum_i R_{\mathbf{A},\mathbf{I}}^i - \sum_{j,i} R_{\mathbf{AV},\mathbf{I}}^{ji} - \sum_{i,j} R_{\mathbf{I},\mathbf{V}}^{ij}, \quad (2.26)$$

$$\frac{\partial C_{\mathbf{V}}}{\partial t} + \operatorname{div} J_{\mathbf{V}} = - \sum_j R_{\mathbf{A},\mathbf{V}}^j - \sum_{i,j} R_{\mathbf{AI},\mathbf{V}}^{ij} - \sum_{i,j} R_{\mathbf{I},\mathbf{V}}^{ij}, \quad (2.27)$$

$$\frac{\partial C_{\mathbf{AI}}}{\partial t} + \operatorname{div} J_{\mathbf{AI}} = \sum_i R_{\mathbf{A},\mathbf{I}}^i - \sum_{i,j} R_{\mathbf{AI},\mathbf{V}}^{ij}, \quad (2.28)$$

$$\frac{\partial C_{\mathbf{AV}}}{\partial t} + \operatorname{div} J_{\mathbf{AV}} = \sum_j R_{\mathbf{A},\mathbf{V}}^j - \sum_{j,i} R_{\mathbf{AV},\mathbf{I}}^{ji}, \quad (2.29)$$

$$\frac{\partial C_{\mathbf{A}}^q}{\partial t} = - \sum_i R_{\mathbf{A},\mathbf{I}}^i - \sum_j R_{\mathbf{A},\mathbf{V}}^j + \sum_{i,j} R_{\mathbf{AI},\mathbf{V}}^{ij} + \sum_{j,i} R_{\mathbf{AV},\mathbf{I}}^{ji}, \quad (2.30)$$

and the Poisson equation

$$-U_T \Delta \ln \left(\frac{n}{n_i} \right) = \frac{e}{\varepsilon} \left(-n + p + qC_{\mathbf{A}}^q + \mathcal{B}_{\mathbf{I}}(n)C_{\mathbf{I}} + \mathcal{B}_{\mathbf{V}}(n)C_{\mathbf{V}} + \mathcal{B}_{\mathbf{AI}}(n)C_{\mathbf{AI}} + \mathcal{B}_{\mathbf{AV}}(n)C_{\mathbf{AV}} \right). \quad (2.31)$$

Applying (2.21), summation over the reaction terms yields in terms of the total concentrations the following concrete expressions:

- dopant–defect pairing:

$$\begin{aligned}
\sum_{i=-1}^{+1} R_{A,I}^i &= \frac{\sum_i k_{A,I}^i K_I^i \left(\frac{n}{n_I}\right)^{-i}}{\sum_i K_I^i \left(\frac{n}{n_I}\right)^{-i}} C_A^q C_I - \frac{\sum_i \tilde{k}_{A,I}^i K_{AI}^{q+i} \left(\frac{n}{n_I}\right)^{-q-i}}{\sum_i K_{AI}^{q+i} \left(\frac{n}{n_I}\right)^{-q-i}} C_{AI} \\
&=: C_I(n) C_A^q C_I - \tilde{C}_I(n) C_{AI}, \tag{2.32}
\end{aligned}$$

$$\begin{aligned}
\sum_{j=-2}^{+2} R_{A,V}^j &= \frac{\sum_j k_{A,V}^j K_V^j \left(\frac{n}{n_I}\right)^{-j}}{\sum_j K_V^j \left(\frac{n}{n_I}\right)^{-j}} C_A^q C_V - \frac{\sum_j \tilde{k}_{A,V}^j K_{AV}^{q+j} \left(\frac{n}{n_I}\right)^{-q-j}}{\sum_j K_{AV}^{q+j} \left(\frac{n}{n_I}\right)^{-q-j}} C_{AV} \\
&=: C_V(n) C_A^q C_V - \tilde{C}_V(n) C_{AV}, \tag{2.33}
\end{aligned}$$

• defect recombination:

$$\begin{aligned}
\sum_{i=-1}^{+1} \sum_{j=-2}^{+2} R_{AI,V}^{ij} &= \frac{\sum_i \sum_j k_{AI,V}^{(q+i)j} K_{AI}^{q+i} K_V^j \left(\frac{n}{n_I}\right)^{-q-i-j}}{\sum_i K_{AI}^{q+i} \left(\frac{n}{n_I}\right)^{-q-i} \sum_j K_V^j \left(\frac{n}{n_I}\right)^{-j}} C_{AI} C_V \\
&\quad - \sum_{i=-1}^{+1} \sum_{j=-2}^{+2} \tilde{k}_{AI,V}^{(q+i)j} \left(\frac{n}{n_I}\right)^{-i-j} C_A^q, \\
&=: D_V(n) C_{AI} C_V - \tilde{D}_V(n) C_A^q, \tag{2.34}
\end{aligned}$$

$$\begin{aligned}
\sum_{j=-2}^{+2} \sum_{i=-1}^{+1} R_{AV,I}^{ji} &= \frac{\sum_j \sum_i k_{AV,I}^{(q+j)i} K_{AV}^{q+j} K_I^i \left(\frac{n}{n_I}\right)^{-q-i-j}}{\sum_j K_{AV}^{q+j} \left(\frac{n}{n_I}\right)^{-q-j} \sum_i K_I^i \left(\frac{n}{n_I}\right)^{-i}} C_{AV} C_I \\
&\quad - \sum_{j=-2}^{+2} \sum_{i=-1}^{+1} \tilde{k}_{AV,I}^{(q+j)i} \left(\frac{n}{n_I}\right)^{-i-j} C_A^q, \\
&=: D_I(n) C_{AV} C_I - \tilde{D}_I(n) C_A^q, \tag{2.35}
\end{aligned}$$

• Frenkel pairs:

$$\begin{aligned}
\sum_{i=-1}^{+1} \sum_{j=-2}^{+2} R_{I,V}^{ij} &= \frac{\sum_i \sum_j k_{I,V}^{ij} K_I^i K_V^j \left(\frac{n}{n_I}\right)^{-i-j}}{\sum_i K_I^i \left(\frac{n}{n_I}\right)^{-i} \sum_j K_V^j \left(\frac{n}{n_I}\right)^{-j}} C_I C_V \\
&\quad - \sum_{i=-1}^{+1} \sum_{j=-2}^{+2} \tilde{k}_{I,V}^{ij} \left(\frac{n}{n_I}\right)^{-i-j}, \\
&=: \mathcal{E}_{IV}(n) C_I C_V - \tilde{\mathcal{E}}_{IV}(n). \tag{2.36}
\end{aligned}$$

Reducing the numbers of parameters we follow the approach of [7], i.e., we express the backward reaction–rate coefficients in terms of the forward ones and the equilibrium ratios $(C_A^q/C_{AI})^*$ and $(C_A^q/C_{AV})^*$ as well as the concentrations of the equilibrium defects C_I^* and C_V^* . These quantities will be specified below.

The averaged reverse reaction–rate constants for the dopant–defect pairings (2.32) and (2.33) result in

$$\tilde{C}_I(n) = C_I(n) C_I^* \left(\frac{C_A^q}{C_{AI}} \right)^* \quad (2.37)$$

and

$$\tilde{C}_V(n) = C_V(n) C_V^* \left(\frac{C_A^q}{C_{AV}} \right)^*. \quad (2.38)$$

The defect recombinations (2.34) and (2.35) yield

$$\tilde{D}_V(n) = D_V(n) C_V^* \left(\frac{C_{AI}}{C_A^q} \right)^*, \quad (2.39)$$

$$\tilde{D}_I(n) = D_I(n) C_I^* \left(\frac{C_{AV}}{C_A^q} \right)^*, \quad (2.40)$$

whereas the reaction term of the Frenkel pairs (2.36) reads as in the intrinsic case

$$\tilde{\mathcal{E}}_{IV}(n) = \mathcal{E}_{IV}(n) C_I^* C_V^*. \quad (2.41)$$

The electrons n obey the Boltzmann statistics

$$n = n_i \exp\left(\frac{e\psi}{k_B T}\right), \quad (2.42)$$

ψ denotes the electrostatic potential. In analogy we have for the holes p

$$p = n_i \exp\left(-\frac{e\psi}{k_B T}\right). \quad (2.43)$$

From (2.42) and (2.43) it follows that $n_i = (np)^{1/2}$ and

$$\psi = U_T \ln\left(\frac{n}{n_i}\right). \quad (2.44)$$

Using (2.37)–(2.44) we end up with the final system of equations in terms of the electrostatic potential, i.e.

$$\begin{aligned}
\frac{\partial C_I}{\partial t} - \operatorname{div} \left[\mathcal{A}_I(\psi) \left(\nabla C_I + \mathcal{B}_I(\psi) C_I \nabla \left(\frac{\psi}{U_T} \right) \right) \right] = \\
- \mathcal{C}_I(\psi) \left(C_A^q C_I - C_I^* \left(\frac{C_A^q}{C_{AI}} \right)^* C_{AI} \right) \\
- \mathcal{D}_I(\psi) \left(C_{AV} C_I - C_I^* \left(\frac{C_{AV}}{C_A^q} \right)^* C_A^q \right) \\
- \mathcal{E}_{IV}(\psi) \left(C_I C_V - C_I^* C_V^* \right), \tag{2.45}
\end{aligned}$$

$$\begin{aligned}
\frac{\partial C_V}{\partial t} - \operatorname{div} \left[\mathcal{A}_V(\psi) \left(\nabla C_V + \mathcal{B}_V(\psi) C_V \nabla \left(\frac{\psi}{U_T} \right) \right) \right] = \\
- \mathcal{C}_V(\psi) \left(C_A^q C_V - C_V^* \left(\frac{C_A^q}{C_{AV}} \right)^* C_{AV} \right) \\
- \mathcal{D}_V(\psi) \left(C_{AI} C_V - C_V^* \left(\frac{C_{AI}}{C_A^q} \right)^* C_A^q \right) \\
- \mathcal{E}_{IV}(\psi) \left(C_I C_V - C_I^* C_V^* \right), \tag{2.46}
\end{aligned}$$

$$\begin{aligned}
\frac{\partial C_{AI}}{\partial t} - \operatorname{div} \left[\mathcal{A}_{AI}(\psi) \left(\nabla C_{AI} + \mathcal{B}_{AI}(\psi) C_{AI} \nabla \left(\frac{\psi}{U_T} \right) \right) \right] = \\
+ \mathcal{C}_I(\psi) \left(C_A^q C_I - C_I^* \left(\frac{C_A^q}{C_{AI}} \right)^* C_{AI} \right) \\
- \mathcal{D}_V(\psi) \left(C_{AI} C_V - C_V^* \left(\frac{C_{AI}}{C_A^q} \right)^* C_A^q \right), \tag{2.47}
\end{aligned}$$

$$\begin{aligned}
\frac{\partial C_{AV}}{\partial t} - \operatorname{div} \left[\mathcal{A}_{AV}(\psi) \left(\nabla C_{AV} + \mathcal{B}_{AV}(\psi) C_{AV} \nabla \left(\frac{\psi}{U_T} \right) \right) \right] = \\
+ \mathcal{C}_V(\psi) \left(C_A^q C_V - C_V^* \left(\frac{C_A^q}{C_{AV}} \right)^* C_{AV} \right) \\
- \mathcal{D}_I(\psi) \left(C_{AV} C_I - C_I^* \left(\frac{C_{AV}}{C_A^q} \right)^* C_A^q \right), \tag{2.48}
\end{aligned}$$

$$\begin{aligned}
\frac{\partial C_A^q}{\partial t} = & - \mathcal{C}_I(\psi) \left(C_A^q C_I - C_I^* \left(\frac{C_A^q}{C_{AI}} \right)^* C_{AI} \right) \\
& - \mathcal{C}_V(\psi) \left(C_A^q C_V - C_V^* \left(\frac{C_A^q}{C_{AV}} \right)^* C_{AV} \right) \\
& + \mathcal{D}_V(\psi) \left(C_{AI} C_V - C_V^* \left(\frac{C_{AI}}{C_A^q} \right)^* C_A^q \right)
\end{aligned}$$

$$+ \mathcal{D}_I(\psi) \left(C_{AV} C_I - C_I^* \left(\frac{C_{AV}}{C_A^q} \right)^* C_A^q \right), \quad (2.49)$$

and the Poisson equation

$$\begin{aligned} \varepsilon \Delta \psi = -e \left(-2n_i \sinh(\psi) + qC_A^q + \mathcal{B}_I(\psi) C_I + \mathcal{B}_V(\psi) C_V \right. \\ \left. + \mathcal{B}_{AI}(\psi) C_{AI} + \mathcal{B}_{AV}(\psi) C_{AV} \right). \end{aligned} \quad (2.50)$$

Now we have to supply equations (2.45)–(2.50) with boundary and initial conditions. The conditions which complete our system of equations depend strongly on the concrete process situation. A precise and for different situations elaborated description of these data can be found in [11]. We assume an implanted dopant profile and take for the interstitials and vacancies at the surface of the wafer the equilibrium concentrations $C_I = C_I^*$ and $C_V = C_V^*$. At *all other boundaries* homogeneous flux conditions are used. For the pairs we simply have homogeneous flux conditions at *all boundaries*. The Poisson equation is equipped with $\psi = 0$ at the *bottom* of the wafer and zero flux conditions *otherwise*.

Appropriate *initial conditions* for the system are given by

$$C_I(\vec{x}, 0) = C_I^*(\vec{x}) \quad \text{and} \quad C_V(\vec{x}, 0) = C_V^*(\vec{x})$$

for the defects, as well as

$$C_{AI}(\vec{x}, 0) = C_{AI}^B \quad \text{and} \quad C_{AV}(\vec{x}, 0) = C_{AV}^B$$

for the pairs, where C_{AI}^B and C_{AV}^B are constant background dopings of order $\mathcal{O}(10^8)$ for instance. The phosphorus concentration is initially set to

$$C_A^q(\vec{x}, 0) = G(\vec{x}),$$

where G is a Gaussian profil ($\max_{\vec{x}} C_A^q(\vec{x}, 0) \gg n_i$), which will be specified in the numerical part.

We remark that Gaussian profiles are just rough approximations of the experimental measured initial distributions of the dopants, since the channeling effects in the lower concentration areas are not regarded, see [5]. Even the frequently used Pearson–IV–distribution is too steep for lower concentration values.

2.2 The Equilibrium Concentrations

The formulations (2.37)–(2.41) of the reverse reaction–rate constants in terms of the forward ones create the parameters

$$\left(\frac{C_A^q}{C_{AI}} \right)^* \quad \text{and} \quad \left(\frac{C_A^q}{C_{AV}} \right)^*.$$

We examine as in [7] the dependence of these quantities on the electrostatic potential. We use (2.32) and (2.37) to get under equilibrium conditions

$$\left(\frac{C_A^q}{C_{AI}}\right)^* = \frac{C_A^q C_I}{C_{AI} C_I^*}.$$

From the intrinsic case, where $n = n_i$, we get

$$\left(\frac{C_A^q}{C_{AI}}\right)^*_{|n=n_i} = \frac{C_{A|n=n_i}^q C_{I|n=n_i}}{C_{AI|n=n_i} C_{I|n=n_i}^*}.$$

Dividing the last two equations gives

$$\left(\frac{C_A^q}{C_{AI}}\right)^* = \left(\frac{C_A^q}{C_{AI}}\right)^*_{|n=n_i} \frac{C_{AI|n=n_i}}{C_{AI}} \frac{C_I}{C_{I|n=n_i}} \frac{C_A^q}{C_{A|n=n_i}^q} \frac{C_{I|n=n_i}^*}{C_I^*}.$$

The use of (2.20) results in

$$\left(\frac{C_A^q}{C_{AI}}\right)^* = \left(\frac{C_A^q}{C_{AI}}\right)^*_{|n=n_i} \frac{\sum_i K_{AI}^{q+i}}{\sum_i K_{AI}^{q+i} \left(\frac{n}{n_i}\right)^{-i}}.$$

An analogous expression can be obtained for $(C_A^q/C_{AV})^*$. The constant quantities

$$(C_A^q/C_{AI})^*_{|n=n_i} \quad \text{and} \quad (C_A^q/C_{AV})^*_{|n=n_i}$$

for the intrinsic conditions are well-known parameters.

From (2.20) we get expressions for the equilibrium constants

$$C_I^* = C_{I|n=n_i}^* \frac{\sum_i K_I^i \left(\frac{n}{n_i}\right)^{-i}}{\sum_i K_I^i}, \quad (2.51)$$

and

$$C_V^* = C_{V|n=n_i}^* \frac{\sum_j K_V^j \left(\frac{n}{n_i}\right)^{-j}}{\sum_j K_V^j}, \quad (2.52)$$

where from (2.44)

$$\left(\frac{n}{n_i}\right) = \exp\left(\frac{\psi}{U_T}\right).$$

Therefore, the initial conditions of the defects result in

$$C_I(\vec{x}, 0) = C_I^*(\psi(\vec{x}, 0)) \quad \text{and} \quad C_V(\vec{x}, 0) = C_V^*(\psi(\vec{x}, 0)),$$

where we use the approximation

$$\psi(\vec{x}, 0) \approx \text{Arsinh}\left(\frac{C_A^q(\vec{x}, 0)}{2n_i}\right).$$

3 The Numerical Treatment

3.1 Numerical Method

The equations (2.45)–(2.50) are a special case of nonlinear reaction–diffusion problems of the form

$$\begin{aligned}
 H(\vec{x}, t, \vec{u}) \vec{u}_t &= \operatorname{div} (D(\vec{x}, t, \vec{u}) \nabla \vec{u}) + \vec{F}(\vec{x}, t, \vec{u}, \nabla \vec{u}), \\
 \vec{x} &\in \Omega, t > 0, \\
 0 &= \xi_1(\vec{x}, t, \vec{u}), \vec{x} \in \partial\Omega_{\mathcal{D}}, \\
 \vec{n}^T D(\vec{x}, t, \vec{u}) \nabla \vec{u} &= \xi_2(\vec{x}, t, \vec{u}), \vec{x} \in \partial\Omega_{\mathcal{C}}, \\
 \vec{u}(\vec{x}, 0) &= \vec{u}_0(\vec{x}), \vec{x} \in \Omega,
 \end{aligned} \tag{3.1}$$

where \vec{u} is the m -dimensional vector of dependent variables. This system is quite general and may consist of parabolic and elliptic differential equations as well as ordinary and algebraic equations when H or D are singular. The nonlinear vector F describes the interaction of all components and allows us to include mild convection. Suitable initial and boundary conditions have to be chosen.

In [13] a time–space adaptive method for the solution of (3.1) has been described in a general setting. This approach aims at an efficient control of time and space grids in such a way that the solution is as accurate as required by the user and the necessary work to get such a solution is minimized.

In the following we first specify the functions involved in (3.1) for our case. Then we recall some essential features of the applied adaptive approach. In the present application the function \vec{u} is a vector of six unknowns:

$$\vec{u} = (C_{\mathcal{I}}, C_{\mathcal{V}}, C_{\mathcal{AI}}, C_{\mathcal{AV}}, C_{\mathcal{A}}^q, \psi). \tag{3.2}$$

The matrix H is diagonal and constant, and has one zero entry

$$H = \operatorname{diag} (1, 1, 1, 1, 1, 0). \tag{3.3}$$

Setting $\vec{d} := \operatorname{div} (D \operatorname{grad} \vec{u})$ we get for the components of \vec{d}

$$d_i = \begin{cases} D_i \nabla u_i + M_i \nabla \psi, & i = 1, 2, 3, 4, \\ 0, & i = 5, \\ \varepsilon, & i = 6. \end{cases} \tag{3.4}$$

where $D_i = D_i(\psi)$ and $M_i = M_i(u_i, \psi)$ are the diffusion coefficients of the concentration and the electrostatic potential ψ with respect to the i th equation. The dielectric constant is denoted by ε . The vector F only depends on the solution vector \vec{u} . Due to the ψ –dependence of $C_{\mathcal{I}}^*$ and $C_{\mathcal{V}}^*$, which we deduced in (2.51) and (2.52), we have to include nonlinear Dirichlet boundary conditions of the form $u_i - u_i^* = 0$ for the $C_{\mathcal{I}}$ and $C_{\mathcal{V}}$ at the surface of the wafer. Homogeneous Dirichlet and Neumann conditions are taken otherwise. Note that no boundary conditions occur for $C_{\mathcal{A}}^q$.

The principle difficulties in numerically solving the above equations are the nonlinearities and the differential–algebraic structure making the system very stiff. Such problems request an implicit or semi–implicit time discretization. Applying a linearly implicit method of Rosenbrock type with automatic step size control, we are able to integrate the system efficiently. Within this approach, the approximate solution \vec{u}_n at time t_n is constructed by a linear combination of the previous solution \vec{u}_{n-1} at time t_{n-1} and different intermediate values $\vec{K}_j^n, j=1, \dots, s$, namely

$$\vec{u}_n = \vec{u}_{n-1} + \sum_{j=1}^s b_j \vec{K}_j^n. \quad (3.5)$$

We employ a third order method with $s = 3$ which has shown to give very satisfactory results for stiff equations [12].

Defining $\vec{f}(\vec{u}) := \vec{d}(\vec{u}) + \vec{F}(\vec{u})$ we formally get a differential–algebraic system

$$H\vec{u}_t = \vec{f}(\vec{u}), \quad \vec{u}(0) = \vec{u}_0.$$

The values $\vec{K}_j^n, j=1, 2, 3$, in (3.5) can now be determined by linear problems

$$\left(\frac{1}{\gamma\tau_n} H - Jf(\vec{u}_{n-1}) \right) \vec{K}_j^n = \vec{f}(\vec{u}_{n-1}) + \sum_{i=1}^{j-1} a_{ji} \vec{K}_i^n + \frac{1}{\tau_n} H \sum_{i=1}^{j-1} c_{ji} \vec{K}_i^n, \quad (3.6)$$

where $\tau_n = t_{n+1} - t_n$ and Jf denotes the Jacobian matrix $\partial\vec{f}/\partial\vec{u}$. The coefficients γ, a_{ji}, c_{ji} , and b_j are chosen such that the method reaches order three and has good stability properties [19]. To get the right boundary conditions for each component of \vec{K}_j^n , the Rosenbrock scheme must be also applied to the algebraic equations describing the solution at the boundary. Note that the solution process for the intermediate values \vec{K}_j^n can be done successively because the sums in the right–hand side of (3.6) extend to $j-1$ only.

The specific structure of the employed Rosenbrock method (3.5) allows us to construct a solution of second order using a simple embedding strategy:

$$\vec{u}_n^* = \vec{u}_{n-1} + \sum_{j=1}^s b_j^* \vec{K}_j^n, \quad (3.7)$$

with a different set of coefficients b_j^* . The difference between the two solutions $\|\vec{u}_n - \vec{u}_n^*\| =: \varepsilon_n$ represent satisfactory estimates the local error of the time discretization and can be utilized to propose a new time step

$$\tau_{n+1} = \frac{\tau_n}{\tau_{n-1}} \left(\frac{TOL_t \varepsilon_{n-1}}{\varepsilon_n \varepsilon_n} \right)^{1/3} \tau_n. \quad (3.8)$$

This step size selection guarantees that the solution is computed with respect to a tolerance TOL_t prescribed by the user [10].

The problems (3.6) equipped with boundary conditions have to be solved for each intermediate value \vec{K}_j^n . In the spirit of full adaptivity we use a self-adaptive multilevel finite element method. Replacing the solution space by an appropriate sequence of discrete spaces with successively increasing dimensions, the size of the arising linear systems necessary to achieve a prescribed accuracy in space can be drastically reduced with respect to uniform methods [2].

The starting point of the finite element method is the weak formulation of (3.6). Let Ω_h be a permissible triangulation of Ω into triangles and let S_h^1 consists of all continuous vector functions the components of which are polynomials of first order on each triangle. Then the finite element solutions $\vec{K}_{j,h}^n \in S_h^1, j=1, 2, 3$, have to satisfy the equations

$$(L_n \vec{K}_{j,h}^n, \vec{\phi}) = (\vec{r}_j^n, \vec{\phi}) \quad \forall \vec{\phi} \in S_h^1, \quad (3.9)$$

where L_n is the weak representation of the differential operator at the left-hand side in (3.6) and includes the boundary conditions. The vector $\vec{r}_j^n = \vec{r}_j^n(\vec{K}_{1,h}^n, \dots, \vec{K}_{j-1,h}^n)$ stand for the whole right-hand side of the j th equation in (3.6). The operator L_n is independent of j , so that the method requires its calculation only once within each time step.

To determine where spatial refinements are necessary and coarse meshes are sufficient, we compute a posteriori error estimates. The goal is to capture local discretization errors involving all variables of the model equations. Here special engineering knowledge about physical properties is not needed. We solve local Dirichlet problems on small subdomains to get a posteriori error estimates. Let Q_w be the set of all quadratic polynomials over w which is the union of two triangles having one common edge. Local approximations \vec{e}_j^n of the spatial errors $\vec{K}_j^n - \vec{K}_{j,h}^n$ are now computed with the basis functions of Q_w . Imposing homogeneous Dirichlet boundary conditions, the local approximate error related to one w is represented by one degree of freedom at the midpoint of the corresponding edge

$$\begin{aligned} (L_n \vec{e}_j^n, \vec{q}) &= (\vec{R}_j^n, \vec{q}) \quad \forall \vec{q} \in Q_w, \vec{x} \in w, \\ \vec{e}_{j,h}^n &= 0, \quad \vec{x} \in \partial w, \\ \vec{R}_j^n &= \vec{r}_j^n(\vec{e}_1^n + \vec{K}_{1,h}^n, \dots, \vec{e}_{j-1}^n + \vec{K}_{j-1,h}^n) - L_n \vec{K}_{j,h}^n. \end{aligned} \quad (3.10)$$

Equipped with these local errors of the intermediate values \vec{K}_j^n , we can form error norms by

$$\|\vec{e}_n\| = \|P \vec{u}_{n-1} + \sum_{j=1}^3 b_j \vec{e}_j^n\|. \quad (3.11)$$

The first contribution $P \vec{u}_{n-1}$ results from the fact that within an adaptive approach the grids for \vec{u}_{n-1} and \vec{u}_n in general are different. The fine grid components of \vec{u}_{n-1} cannot be represented on those parts of the current grid where the latter is coarser than the grid of the previous time step. So, we get an additional projection error $P \vec{u}_{n-1}$.

We can form both local and global error informations taking Ω_h or w to compute the norms in (3.11), for use in our adaptive mesh control algorithm. Local a posteriori error estimates are employed to decide which elements to refine or to unrefine. For refinement

a marked triangle is divided into four congruent triangles ('red' refinement). After that triangles with two or three refined edges are compulsorily refined 'red'; triangles with only one refined edge are subdivided into two triangles ('green' closure). These 'green' elements are removed in a next refinement step to avoid bad geometric properties of the triangulation. This refinement strategy is standard and used e.g. in the KASKADE code [4]. Coarsening takes place only after an accepted time step before starting the multilevel process. Employing the asymptotic behaviour of the local errors, we predict the error after coarsening and remove elements whenever the predicted error is still above the refinement barrier. Doing this we have the justified hope that the new region will be not immediately refined in the next time step.

The aim of our mesh adaptation is to equilibrate the error until a final mesh is created in which all elements have approximately the same error, and a global prescribed tolerance TOL_x is reached. The relationship between spatial and temporal accuracy is studied in [14]. Given a prescribed tolerance TOL we set

$$TOL_x = TOL/3.0 \quad \text{and} \quad TOL_t = TOL/2.0.$$

The linear systems are solved by the BICGStab–algorithm [20] preconditioned with an ILU–method.

3.2 The Physical Parameters

We have solved the dopant diffusion process in two spatial dimensions on the rectangle

$$\Omega = \{\vec{x} = (x_1, x_2) \in \mathbb{R}^2, 0 < x_1 < 10^{-3}, 0 < x_2 < 10^{-4}\}$$

for $t > 0$, where the unit of measurement is given in cm. So, the wafer surface is at $x_1 = 0$ and the bottom is at $x_1 = 10^{-3}$. The expansion of the computational domain guarantees that the solution is not affected by the boundary condition at the bottom.

The implanted phosphorus concentration has been set initially to the Gaussian profile

$$C_A^q(\vec{x}, 0) = \tilde{C}_A^q \exp\left(-\frac{1}{2} \frac{f(\vec{x} - \vec{a})}{\sigma^2}\right),$$

where $\tilde{C}_A^q \gg n_i$ is the maximal value of the function, $\vec{a} = (a_1, a_2)$ determines the position of the profile, σ is the standard deviation and

$$f(\vec{x} - \vec{a}) = (x_1 - a_1)^2 + \frac{1}{4} \left((|x_2 - a_2| - b) + |x_2 - a_2 - b| \right)^2.$$

If $b = 0$, then we have the usual Gaussian profile, for $b > 0$ the maximum extends to a whole line of length b in x_2 –direction. For the simulation we chose

$$\sigma = 0.027 \times 10^{-4} \text{cm}, a_1 = 0.02 \times 10^{-4} \text{cm}, a_2 = 0.5 \times 10^{-4} \text{cm}, b = 1.0 \times 10^{-5} \text{cm}.$$

The model requires an enormous list of parameters. Most of them are essentially unknown or at least controversial. The set of parameters we used in our simulations was taken from [7] and [16] which we summarize in Table 1 and Table 2. The physical parameters listed in Table 1 obey the well-known Arrhenius relation.

Parameter values for Arrhenius' law		
constant	prefactor	energy [eV]
$D_{I n=n_i} [cm^2 s^{-1}]$	2.629×10^{11}	4.436
$D_{V n=n_i} [cm^2 s^{-1}]$	2.639×10^6	4.002
$C_{I n=n_i}^* [cm^{-3}]$	1.132×10^{18}	1.377
$C_{V n=n_i}^* [cm^{-3}]$	1.642×10^{24}	2.226
$D_{AI}^0 [cm^2 s^{-1}]$	8.570×10^{-1}	1.720
$D_{AI}^1 [cm^2 s^{-1}]$	1.780×10^6	3.340
$D_{AI}^2 [cm^2 s^{-1}]$	4.128×10^{-3}	1.330
$D_{AV}^{-1} [cm^2 s^{-1}]$	6.123×10^3	2.550
$D_{AV}^0 [cm^2 s^{-1}]$	5.466×10^5	3.040
$D_{AV}^1 [cm^2 s^{-1}]$	7.094×10^9	4.090
$D_{AV}^2 [cm^2 s^{-1}]$	1.509×10^0	1.840
$D_{AV}^3 [cm^2 s^{-1}]$	1.509×10^0	1.840
K_{AI}^0	1.000×10^0	0.000
K_{AI}^1	1.995×10^6	1.880
K_{AI}^2	4.422×10^{12}	3.020
K_{AV}^{-1}	8.601×10^{13}	3.260
K_{AV}^0	1.000×10^0	0.000
K_{AV}^1	9.501×10^{15}	3.780
K_{AV}^2	7.068×10^3	0.920
K_{AV}^3	1.317×10^{20}	4.760

Table 1.

Note, for the point defects we used for all charge states the intrinsic diffusivities $D_{I|n=n_i}$ and $D_{V|n=n_i}$, which were obtained from experiments via gold diffusion.

The proportionality quantities K_I^z and K_V^z , taken from [16], satisfy

$$K_X^z = \text{prefactor}(z) \exp\left(\frac{\text{value}(z) T}{T + 636}\right) \exp\left(-\frac{\text{energy}(z)}{k_B T}\right),$$

where $X = I, V$ and z denotes the charge states. Table 2 summarizes the precise values.

constant	prefactor	value	energy [eV]
K_I^{-1}	0.754	0.868	0.185
K_I^0	1.000	0.000	0.000
K_I^1	1.326	0.868	0.185
K_V^{-2}	0.569	2.252	0.480
K_V^{-1}	0.754	0.070	0.015
K_V^0	1.000	0.000	0.000
K_V^1	1.326	2.557	0.545
K_V^2	1.758	4.702	1.002

Table 2.

The forward reaction-rate constants $k_{X,Y}^{rs}$ and $k_{A,Y}^s$ ($X, Y = I, V, AI, AV$ and r, s denote the charge states) may be expressed as

$$k_{X,Y}^{rs} = 4\pi r_c (D_X^r + D_Y^s) \exp\left(-\frac{E_{X,Y}^{rs}}{k_B T}\right)$$

and

$$k_{A,Y}^s = 4\pi r_c (D_{A|n=n_i} + D_Y^s) \exp\left(-\frac{E_{A,Y}^s}{k_B T}\right).$$

Therein, r_c denotes the capture radius, which was set equal to 5 Å. All the barrier energies $E_{X,Y}^{rs}$ and $E_{X,Y}^s$ were taken to be zero, except for the Frenkel pair reaction, where we took the value 0.3 eV. The effective intrinsic diffusion coefficient is well-known, i.e., due to [6]

$$D_{A|n=n_i} = 3.850 \times 10^0 \exp\left(-\frac{3.660}{k_B T}\right).$$

In order to complete the discussion concerning the physical parameters, we set

$$(C_A^q/C_{AI})_{|n=n_i}^* = 3.129 \times 10^{16} \exp\left(-\frac{1.680}{k_B T}\right)$$

and compute $(C_A^q/C_{AV})_{|n=n_i}^*$ from the relationship

$$D_{A|n=n_i} = (C_{AI}/C_A^q)_{|n=n_i}^* D_{AI|n=n_i} + (C_{AV}/C_A^q)_{|n=n_i}^* D_{AV|n=n_i},$$

the derivation of which can be found in [7]. Here, we set $D_{AX|n=n_i} = D_{AX}^0$, $X = I, V$.

The tabulated quantities are valid in our case over a temperature range of 900⁰–1200⁰C. Thus the set of parameters is complete.

3.3 The Numerical Simulations

Next we present a series of numerical experiments.

Fig. 1 represents the coarse initial grid of size $10^{-3} \times 10^{-4} \text{ cm}^2$, which will be adaptively refined by the algorithm during the process as already described. Since the effects occurring in the bulk are spread out around $1.0 \text{ }\mu\text{m}$ from the wafer surface (the left hand part of the domain), we cut the domain just for the graphical presentation of the results.

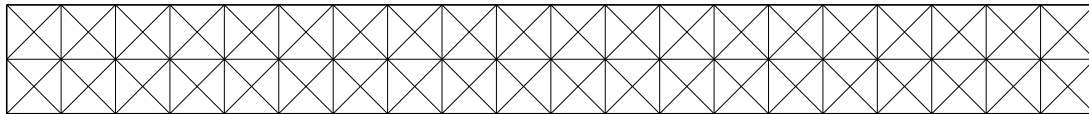


Fig. 1. Initial grid of size $10^{-3} \times 10^{-4} \text{ cm}^2$.

Fig. 2 contains the evolution of diffusion profiles of phosphorus at different time points. Additionally the one dimensional cuts through the centre are shown in order to compare the maximal values of the profiles with respect to time. The phosphorus profile shows its typical “kink and tail” behaviour (anomalous diffusion of phosphorus), a phenomenon about which a detailed discussion can be found in [18].

Fig. 3 illustrates the evolution of the defects. An interesting observation is that the total concentrations of the defects grow very rapidly at the wafer surface. This results from the high concentration of free electrons brought into the bulk by the high implanted phosphorus concentration. Since the neutral portion of the defects becomes charged its concentration decreases near the surface. On the other hand, the defects have to satisfy a Dirichlet boundary condition at the surface, which is constant for the neutral portion during the whole evolution, as can be seen in the picture. A steep gradient is generated in the bulk near the surface, forcing new neutral defects (from somewhere) into the wafer in order to compensate the loss of neutral defects. Thus, the concentrations of the neutral defects, as can be seen in the picture, become constant (the constant is equal to the intrinsic equilibrium value) everywhere in the wafer at time $t = 1.0 \times 10^{-20}$ seconds. As a consequence the total concentration grows at the very next moment at the wafer surface. Let us remark at this point, that the just mentioned redistribution of the defects could be regarded as a possible initial state of them, but then equipped with homogeneous Neumann-conditions at the surface during the whole evolution of the species.

The change from “concave to convex” of the interstitial concentration, which occurs around $t = 10^{-5}$, produces step gradients of the profile and therefore the adaptive algorithm increases the grid points drastically in order to resolve this situation as can be seen in Fig. 6.

